AGU PUBLICATIONS

Journal of Geophysical Research: Solid Earth

Supporting Information for

The effect of faceting on olivine wetting properties

Yongsheng Huang[1, a*], Takayuki Nakatani[1, b], Sando Sawa[1. c], Michihiko Nakamura[1], Catherine McCammon[2]

1. Department of Earth Science, Graduate School of Science, Tohoku University, Aramaki–Aza–Aoba, Aoba–Ku, Sendai, Miyagi 980–8578, Japan

2. Bayerisches Geoinstitut, University of Bayreuth, 95440 Bayreuth, Germany

a. Current address: Guangzhou Institute of Geochemistry, Chinese Academy of Sciences, 511 Kehua Street, Wushan, Tianhe, Guangzhou 510640, China.

b. Current address: Geological Survey of Japan, AIST Central 7, Higashi 1–1–1, Tsukuba, Ibaraki 305–8567, Japan.

c. Current address: Division of Advanced Mechanical Systems Engineering, Institute of Engineering, Tokyo University of Agriculture and Technology, Nakamachi 2-24-16, Koganei, Tokyo, 184-0012, Japan.

* Corresponding author. Email: huangyongsheng@gig.ac.cn

Contents of this file

1. Note 1. Errors of the GBPD analyses

Our GBPD analyses focused on the olivine–olivine–fluid triple junction with apparent dihedral angles lower than the median value + 5° and assumed a vertical grain boundary plane there. Based on the simple theoretical calculation, we show that grain boundary planes at such triple junctions are dominantly subvertical with respect to the polished section. Although we cannot exactly determine the extent of grain boundary plane tilting in the cross-sectional image, the apparent dihedral angles can be used to constrain the extent of tilting statistically.

Following the method of Harker and Parker (1945), we can calculate e apparent dihedral angle, Y on an arbitrary sectioning plane at the mineral–mineral–fluid triple junction in an isotropic system with one true dihedral angle θ. This method is identical to that used to compute the theoretical cumulative frequency curve of the apparent dihedral angle, as shown in Figure 3. A schematic of the triple junction with a sectioning plane is shown in Figure S1. The unit normal of the sectioning plane is defined in angular coordinates Q and ϕ (Q, ϕ = 0–90°), and Y is a function of θ, Q, and ϕ (Harker & Parker, 1945). In Figure S2a, the contours of Y for a representative θ of 60° are shown in the sin2Q versus ϕ diagram. In this diagram, the area fraction of angles ≤ Y corresponds to the probability that the observed apparent dihedral angles become less than, or equal to, Y (Harker & Parker, 1945). The apparent dihedral angles around θ were more likely to be observed on the polished section than the other angles. The median of the Y values closely corresponds to θ (Jurewicz & Jurewicz, 1986). We note that a Y smaller than θ requires a smaller ϕ, and vice versa. Increasing sin2Q (i.e., Q) tends to cause Y values to deviate from the median (i.e., θ).

The angle between the grain boundary plane and the arbitrary sectioning plane, F (F = 0–90°) can be calculated from their normals. F is dependent on Q and f, but independent of θ (Figure S1). In Figure S2b, the contours of F are shown in the sin2Q versus f diagram. As in the case of Y, the area fraction of the angles ≥ F should correspond to the probability that the angles become more than or equal to F. At sin2Q (i.e., Q) = 0 or ϕ = 0, the grain boundary plane is vertical (F = 90°). With increasing Q and ϕ, F tends to deviate from 90°: the grain boundary plane becomes more tilted. Therefore, subvertical (i.e., F close to 90°) grain boundary planes can be expected at the triple junction with Y smaller than the median, because such Y values can only be observed at low ϕ.

Combining the Y and F contours in the sin2Q versus ϕ diagram allows us to compute the probability of observing subvertical grain boundary planes at the triple junctions in an arbitrary Y window on the polished section. We regarded the minimum deviation of F from 90°, which satisfies probability of more than ~68%, as the representative error (1s) of our GBPD analyses. In figure S2c, the area of F ≥ 67° in our preferred Y window from 0° to 65° (i.e., median + 5°) is shown in the sin2Q versus f diagram for θ = 60°. 71% of the apparent dihedral angles fell within the range of 0° ≤ Y ≤ 65° in which 68% of grain boundary planes formed an angle greater than or equal to 67° with respect to the sectioning plane. Thus, we inferred the representative errors of ~23° in our GBPD analyses. Although this value slightly increased and decreased at lower and higher θ, respectively, it was not significantly dependent on θ in the range of interest (23–24° at θ = 50–80°). If we do not use dihedral angle constraints (i.e., Y window of 0–180°), the probability of F ≥ 67° decreases to 49% and the estimated error becomes 35°.

2. Figures S1 to S10. The Supporting Information Figures

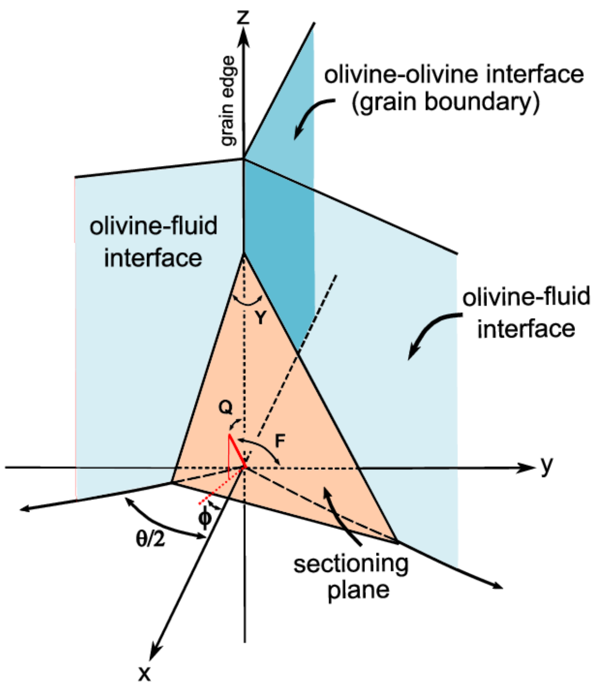

Figure S1. Schematic olivine–olivine–fluid triple junction with a sectioning plane after Jurewicz and Jurewicz (1986). θ is the true dihedral angle formed by two olivine–fluid interfaces (pale blue planes). Y is the apparent dihedral angle observed on the sectioning plane (pale orange plane). The bold red line represents the unit normal of the sectioning plane defined in the angular coordinates Q and ϕ. F is the angle formed by the sectioning plane and grain boundary plane (deep sky–blue plane).

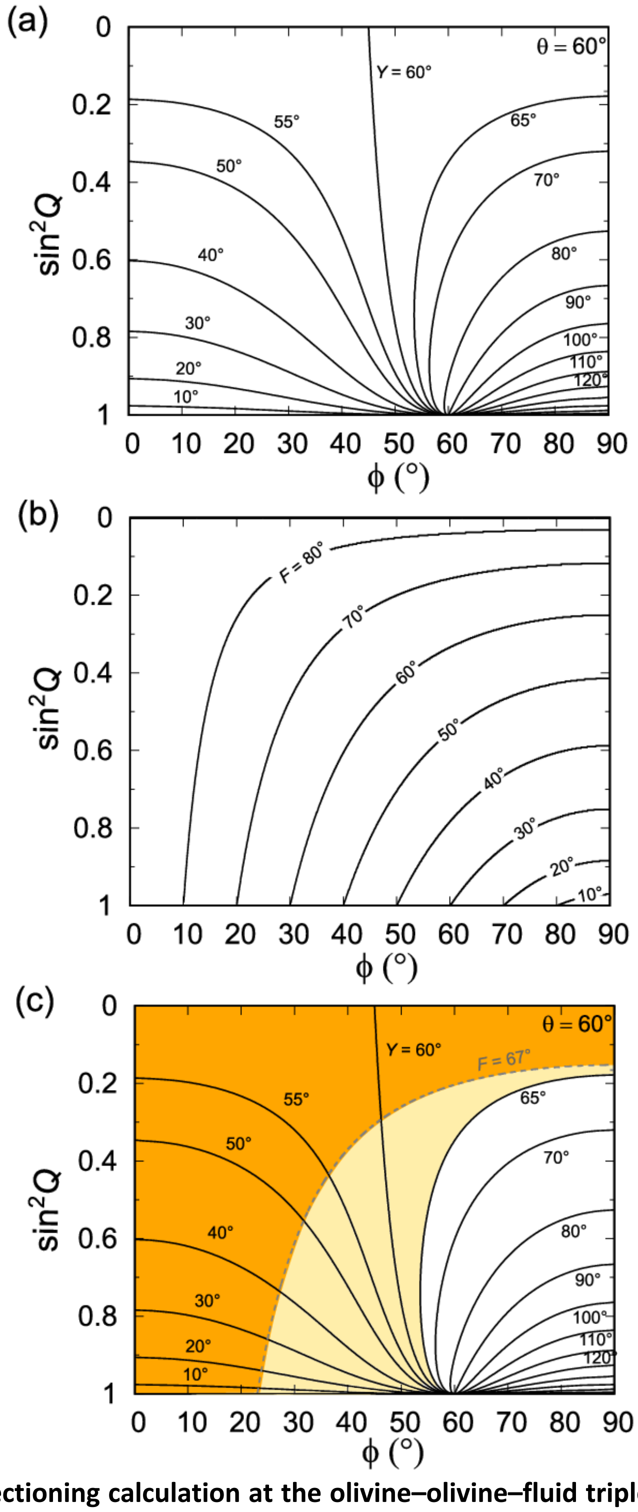

Figure S2. Results of sectioning calculation at the olivine–olivine–fluid triple junction. a, Contours of the apparent dihedral angle, Y in the sin2Q versus ϕ diagram calculated according to Harker and Parker (1945) assuming the true dihedral angle, θ of 60°. **b,** Contours of the angle formed by grain boundary plane and sectioning plane, F in the sin2Q versus ϕ diagram. **c,** The area of F ≥ 67° within the Y window of 0–65° in the sin2Q versus ϕ diagram (orange). The ratio of this area to the area of Y = 0–60° (orange + pale yellow) yields the probability of F ≥ 67° in the selected Y window.

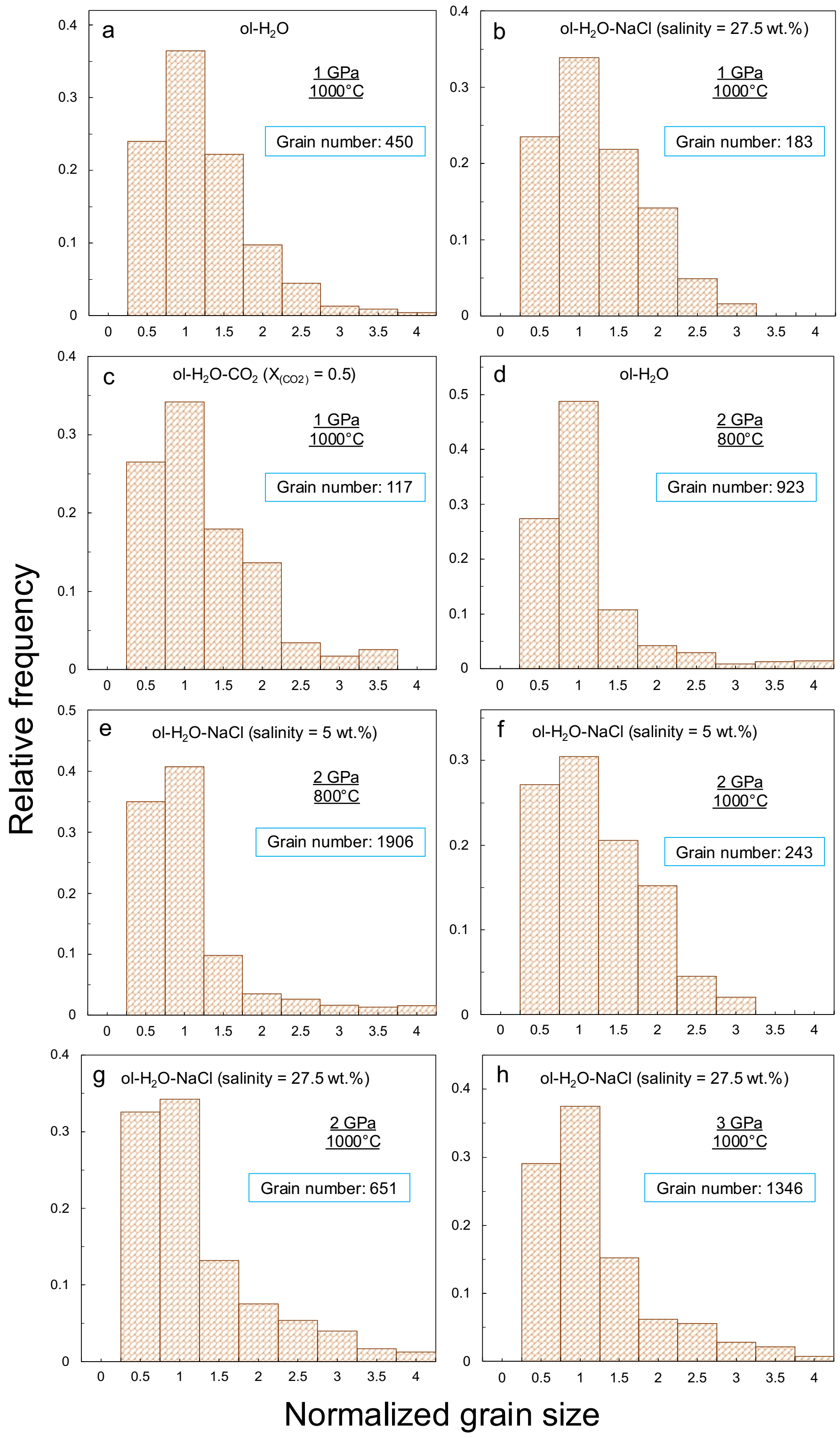

Figure S3. Histogram of the grain size distribution in the olivine–fluid system. The grain size distribution was normalized by the mean grain size of the recovered sample. The grain size is concentrated with a peak around the mean grain size. Abbreviation: ol = olivine.

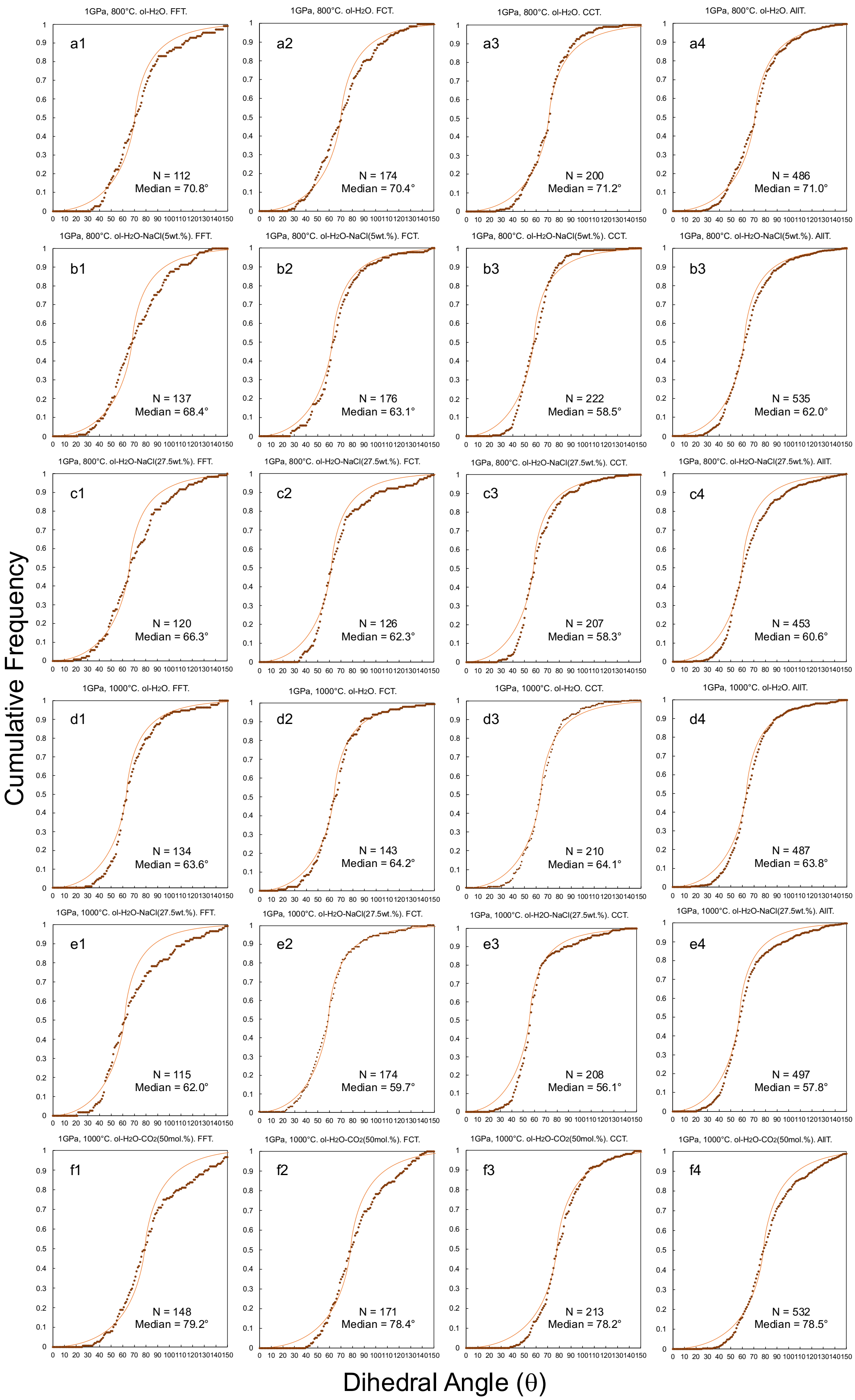
1GPa, 800°C. ol-H2O. FFT.
a1
N = 112
Median = 70.8°
1GPa, 800°C. ol-H2O. FCT.
a2
N = 174
Median = 70.4°
1GPa, 800°C. ol-H2O. CCT.
a3
N = 200
Median = 71.2°
1GPa, 800°C. ol-H2O. AllT.
a4
N = 486
Median = 71.0°
1GPa, 800°C. ol-H2O-NaCl(5wt.%). FFT.
b1
N = 137
Median = 68.4°
1GPa, 800°C. ol-H2O-NaCl(5wt.%). FCT.
b2
N = 176
Median = 63.1°
1GPa, 800°C. ol-H2O-NaCl(5wt.%). CCT.
b3
N = 222
Median = 58.5°
1GPa, 800°C. ol-H2O-NaCl(5wt.%). AllT.
b3
N = 535
Median = 62.0°
1GPa, 800°C. ol-H2O-NaCl(27.5wt.%). FFT.
c1
N = 120
Median = 66.3°
1GPa, 800°C. ol-H2O-NaCl(27.5wt.%). FCT.
c2
N = 126
Median = 62.3°
1GPa, 800°C. ol-H2O-NaCl(27.5wt.%). CCT.
c3
N = 207
Median = 58.3°
1GPa, 800°C. ol-H2O-NaCl(27.5wt.%). AllT.
c4
N = 453
Median = 60.6°
1GPa, 1000°C. ol-H2O. FFT.
d1
N = 134
Median = 63.6°
1GPa, 1000°C. ol-H2O. FCT.
d2
N = 143
Median = 64.2°
1GPa, 1000°C. ol-H2O. CCT.
d3
N = 210
Median = 64.1°
1GPa, 1000°C. ol-H2O. AllT.
d4
N = 487
Median = 63.8°
1GPa, 1000°C. ol-H2O-NaCl(27.5wt.%). FFT.
e1
N = 115
Median = 62.0°
1GPa, 1000°C. ol-H2O-NaCl(27.5wt.%). FCT.
e2
N = 174
Median = 59.7°
1GPa, 1000°C. ol-H2O-NaCl(27.5wt.%). CCT.
e3
N = 208
Median = 56.1°
1GPa, 1000°C. ol-H2O-NaCl(27.5wt.%). AllT.
e4
N = 497
Median = 57.8°
1GPa, 1000°C. ol-H2O-CO2(50mol.%). FFT.
f1
N = 148
Median = 79.2°
1GPa, 1000°C. ol-H2O-CO2(50mol.%). FCT.
f2
N = 171
Median = 78.4°
1GPa, 1000°C. ol-H2O-CO2(50mol.%). CCT.
f3
N = 213
Median = 78.2°
1GPa, 1000°C. ol-H2O-CO2(50mol.%). AllT.
f4
N = 532
Median = 78.5°
Cumulative Frequency
Dihedral Angle (θ)

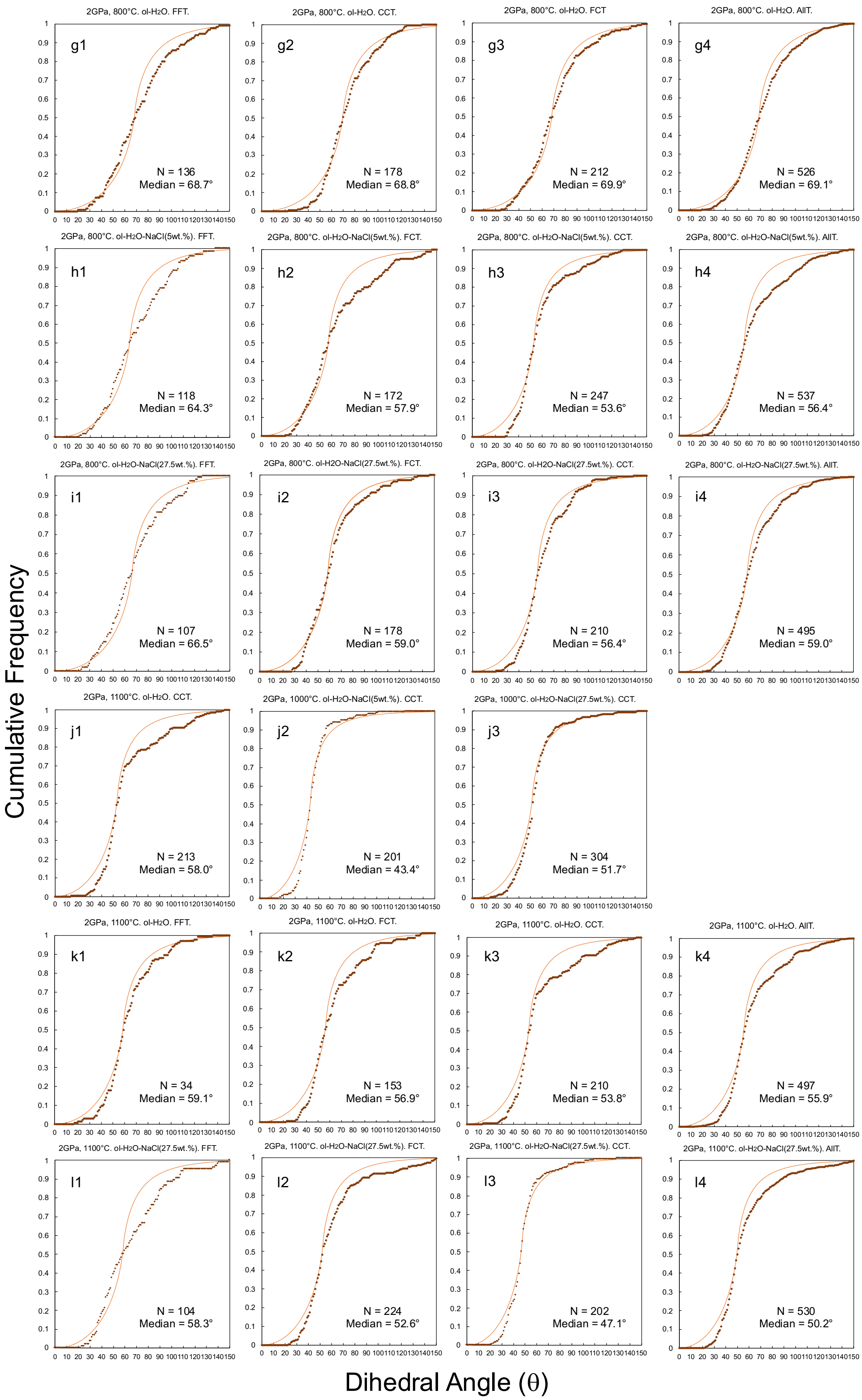
Cumulative Frequency
Dihedral Angle (θ)
2GPa, 800°C. ol-H2O. FFT.
g1
N = 136
Median = 68.7°
2GPa, 800°C. ol-H2O. CCT.
g2
N = 178
Median = 68.8°
2GPa, 800°C. ol-H2O. FCT
g3
N = 212
Median = 69.9°
2GPa, 800°C. ol-H2O. AllT.
g4
N = 526
Median = 69.1°
2GPa, 800°C. ol-H2O-NaCl(5wt.%). FFT.
h1
N = 118
Median = 64.3°
2GPa, 800°C. ol-H2O-NaCl(5wt.%). FCT.
h2
N = 172
Median = 57.9°
2GPa, 800°C. ol-H2O-NaCl(5wt.%). CCT.
h3
N = 247
Median = 53.6°
2GPa, 800°C. ol-H2O-NaCl(5wt.%). AllT.
h4
N = 537
Median = 56.4°
2GPa, 800°C. ol-H2O-NaCl(27.5wt.%). FFT.
i1
N = 107
Median = 66.5°
2GPa, 800°C. ol-H2O-NaCl(27.5wt.%). FCT.
i2
N = 178
Median = 59.0°
2GPa, 800°C. ol-H2O-NaCl(27.5wt.%). CCT.
i3
N = 210
Median = 56.4°
2GPa, 800°C. ol-H2O-NaCl(27.5wt.%). AllT.
i4
N = 495
Median = 59.0°
2GPa, 1100°C. ol-H2O. CCT.
j1
N = 213
Median = 58.0°
2GPa, 1000°C. ol-H2O-NaCl(5wt.%). CCT.
j2
N = 201
Median = 43.4°
2GPa, 1000°C. ol-H2O-NaCl(27.5wt.%). CCT.
j3
N = 304
Median = 51.7°
2GPa, 1100°C. ol-H2O. FFT.
k1
N = 34
Median = 59.1°
2GPa, 1100°C. ol-H2O. FCT.
k2
N = 153
Median = 56.9°
2GPa, 1100°C. ol-H2O. CCT.
k3
N = 210
Median = 53.8°
2GPa, 1100°C. ol-H2O. AllT.
k4
N = 497
Median = 55.9°
2GPa, 1100°C. ol-H2O-NaCl(27.5wt.%). FFT.
l1
N = 104
Median = 58.3°
2GPa, 1100°C. ol-H2O-NaCl(27.5wt.%). FCT.
l2
N = 224
Median = 52.6°
2GPa, 1100°C. ol-H2O-NaCl(27.5wt.%). CCT.
l3
N = 202
Median = 47.1°
2GPa, 1100°C. ol-H2O-NaCl(27.5wt.%). AllT.
l4
N = 530
Median = 50.2°

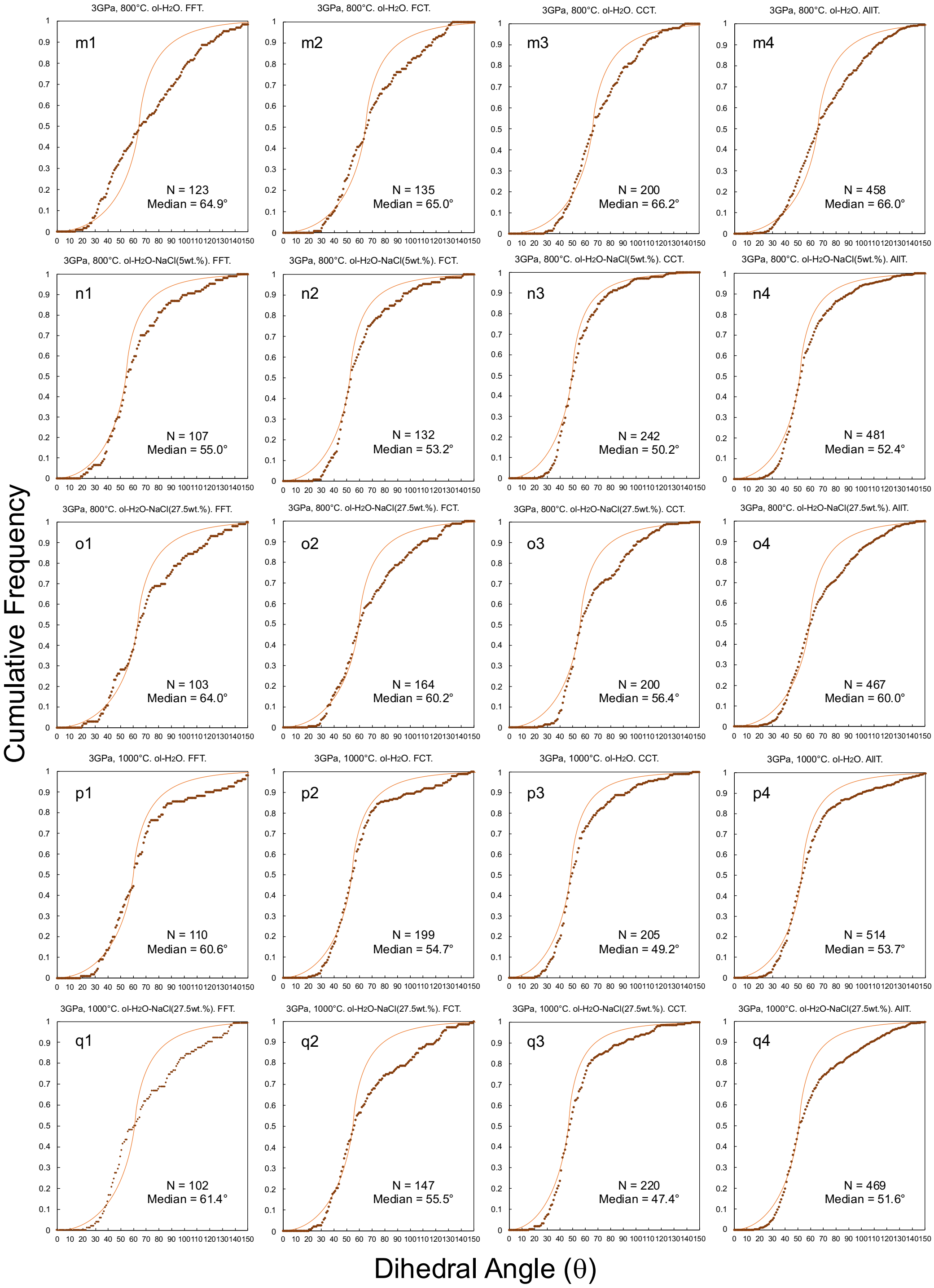

Figure S4. Cumulative frequency curves of measured apparent dihedral angles (θ) in olivine–fluid systems at 1–3 GPa and 800–1100 °C. The median value and number (N) of the measured angles are shown for each experimental condition. The solid lines represent the theoretical cumulative frequency curves of the isotropic system with one true θ (Jurewicz & Jurewicz, 1986). This angle is assumed to coincide with the obtained median value. The P–T and fluid composition are shown for each system. Abbreviations: ol=olivine, FFT = faceted–faceted type angle, FCT = faceted–curved type angle, CCT= curved–curved type angle, AllT= all type of measured angle.

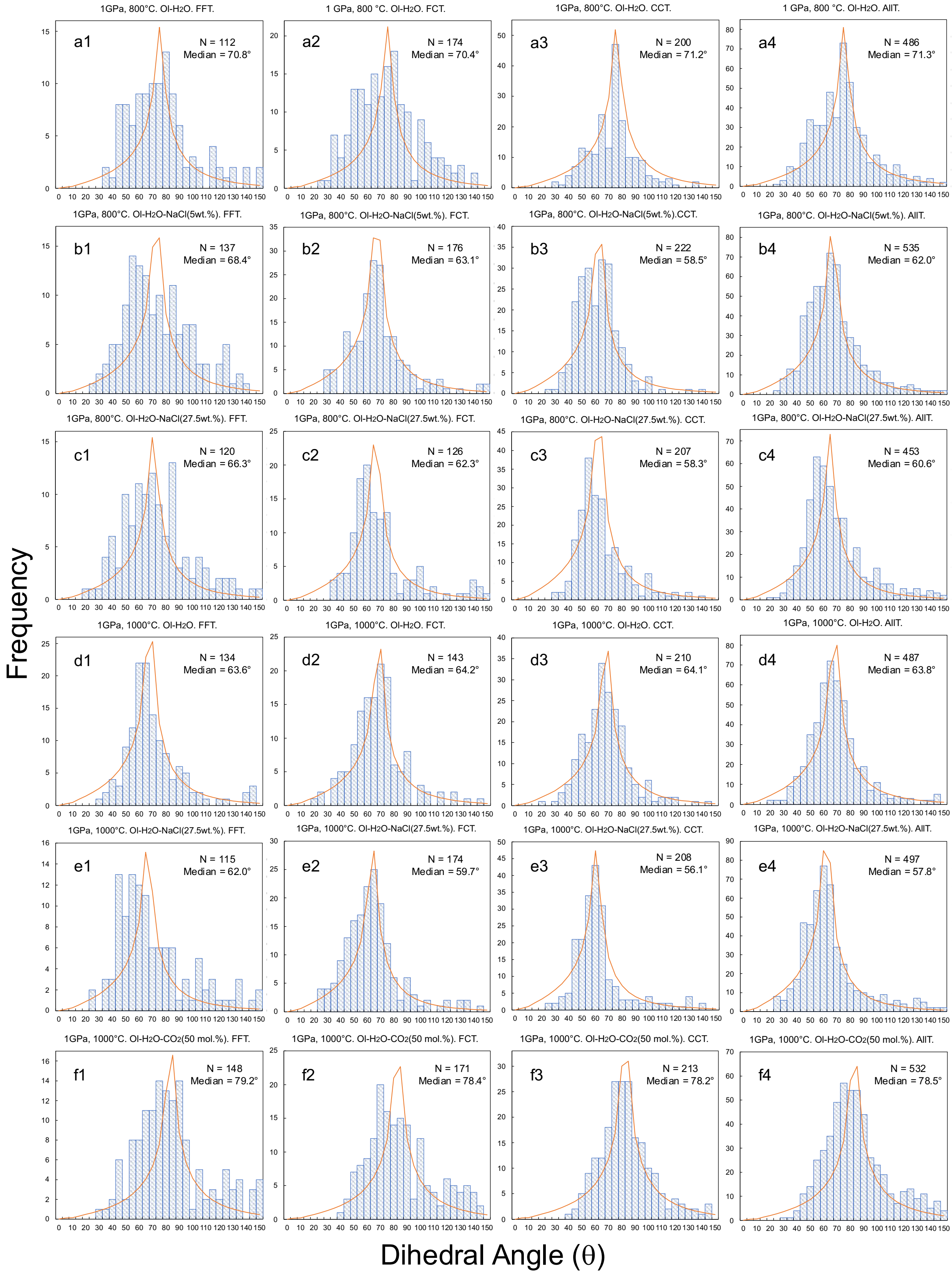

1GPa, 800°C. Ol-H2O. FFT.
a1
N = 112
Median = 70.8°
1 GPa, 800 °C. Ol-H2O. FCT.
a2
N = 174
Median = 70.4°
1GPa, 800°C. Ol-H2O. CCT.
a3
N = 200
Median = 71.2°
1 GPa, 800 °C. Ol-H2O. AllT.
a4
N = 486
Median = 71.3°
1GPa, 800°C. Ol-H2O-NaCl(5wt.%). FFT.
b1
N = 137
Median = 68.4°
1GPa, 800°C. Ol-H2O-NaCl(5wt.%). FCT.
b2
N = 176
Median = 63.1°
1GPa, 800°C. Ol-H2O-NaCl(5wt.%).CCT.
b3
N = 222
Median = 58.5°
1GPa, 800°C. Ol-H2O-NaCl(5wt.%). AllT.
b4
N = 535
Median = 62.0°
1GPa, 800°C. Ol-H2O-NaCl(27.5wt.%). FFT.
c1
N = 120
Median = 66.3°
1GPa, 800°C. Ol-H2O-NaCl(27.5wt.%). FCT.
c2
N = 126
Median = 62.3°
1GPa, 800°C. Ol-H2O-NaCl(27.5wt.%). CCT.
c3
N = 207
Median = 58.3°
1GPa, 800°C. Ol-H2O-NaCl(27.5wt.%). AllT.
c4
N = 453
Median = 60.6°
1GPa, 1000°C. Ol-H2O. FFT.
d1
N = 134
Median = 63.6°
1GPa, 1000°C. Ol-H2O. FCT.
d2
N = 143
Median = 64.2°
1GPa, 1000°C. Ol-H2O. CCT.
d3
N = 210
Median = 64.1°
1GPa, 1000°C. Ol-H2O. AllT.
d4
N = 487
Median = 63.8°
1GPa, 1000°C. Ol-H2O-NaCl(27.5wt.%). FFT.
e1
N = 115
Median = 62.0°
1GPa, 1000°C. Ol-H2O-NaCl(27.5wt.%). FCT.
e2
N = 174
Median = 59.7°
1GPa, 1000°C. Ol-H2O-NaCl(27.5wt.%). CCT.
e3
N = 208
Median = 56.1°
1GPa, 1000°C. Ol-H2O-NaCl(27.5wt.%). AllT.
e4
N = 497
Median = 57.8°
1GPa, 1000°C. Ol-H2O-CO2(50 mol.%). FFT.
f1
N = 148
Median = 79.2°
1GPa, 1000°C. Ol-H2O-CO2(50 mol.%). FCT.
f2
N = 171
Median = 78.4°
1GPa, 1000°C. Ol-H2O-CO2(50 mol.%). CCT.
f3
N = 213
Median = 78.2°
1GPa, 1000°C. Ol-H2O-CO2(50 mol.%). AllT.
f4
N = 532
Median = 78.5°
Frequency
Dihedral Angle (θ)

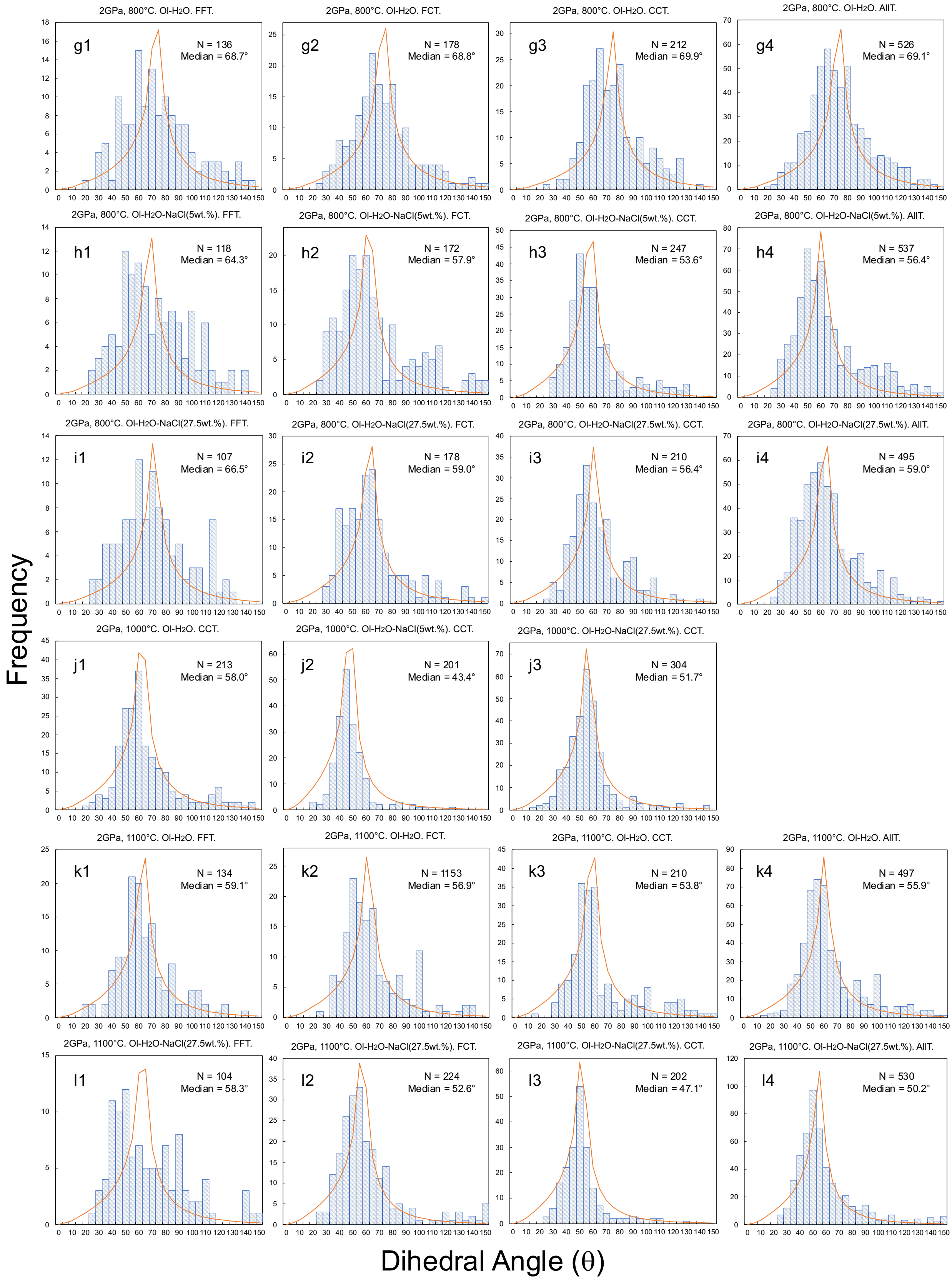

2GPa, 800°C. Ol-H2O. FFT.
g1
N = 136
Median = 68.7°
2GPa, 800°C. Ol-H2O. FCT.
g2
N = 178
Median = 68.8°
2GPa, 800°C. Ol-H2O. CCT.
g3
N = 212
Median = 69.9°
2GPa, 800°C. Ol-H2O. AllT.
g4
N = 526
Median = 69.1°
2GPa, 800°C. Ol-H2O-NaCl(5wt.%). FFT.
h1
N = 118
Median = 64.3°
2GPa, 800°C. Ol-H2O-NaCl(5wt.%). FCT.
h2
N = 172
Median = 57.9°
2GPa, 800°C. Ol-H2O-NaCl(5wt.%). CCT.
h3
N = 247
Median = 53.6°
2GPa, 800°C. Ol-H2O-NaCl(5wt.%). AllT.
h4
N = 537
Median = 56.4°
2GPa, 800°C. Ol-H2O-NaCl(27.5wt.%). FFT.
i1
N = 107
Median = 66.5°
2GPa, 800°C. Ol-H2O-NaCl(27.5wt.%). FCT.
i2
N = 178
Median = 59.0°
2GPa, 800°C. Ol-H2O-NaCl(27.5wt.%). CCT.
i3
N = 210
Median = 56.4°
2GPa, 800°C. Ol-H2O-NaCl(27.5wt.%). AllT.
i4
N = 495
Median = 59.0°
2GPa, 1000°C. Ol-H2O. CCT.
j1
N = 213
Median = 58.0°
2GPa, 1000°C. Ol-H2O-NaCl(5wt.%). CCT.
j2
N = 201
Median = 43.4°
2GPa, 1000°C. Ol-H2O-NaCl(27.5wt.%). CCT.
j3
N = 304
Median = 51.7°
2GPa, 1100°C. Ol-H2O. FFT.
k1
N = 134
Median = 59.1°
2GPa, 1100°C. Ol-H2O. FCT.
k2
N = 1153
Median = 56.9°
2GPa, 1100°C. Ol-H2O. CCT.
k3
N = 210
Median = 53.8°
2GPa, 1100°C. Ol-H2O. AllT.
k4
N = 497
Median = 55.9°
2GPa, 1100°C. Ol-H2O-NaCl(27.5wt.%). FFT.
l1
N = 104
Median = 58.3°
2GPa, 1100°C. Ol-H2O-NaCl(27.5wt.%). FCT.
l2
N = 224
Median = 52.6°
2GPa, 1100°C. Ol-H2O-NaCl(27.5wt.%). CCT.
l3
N = 202
Median = 47.1°
2GPa, 1100°C. Ol-H2O-NaCl(27.5wt.%). AllT.
l4
N = 530
Median = 50.2°
Frequency
Dihedral Angle (θ)

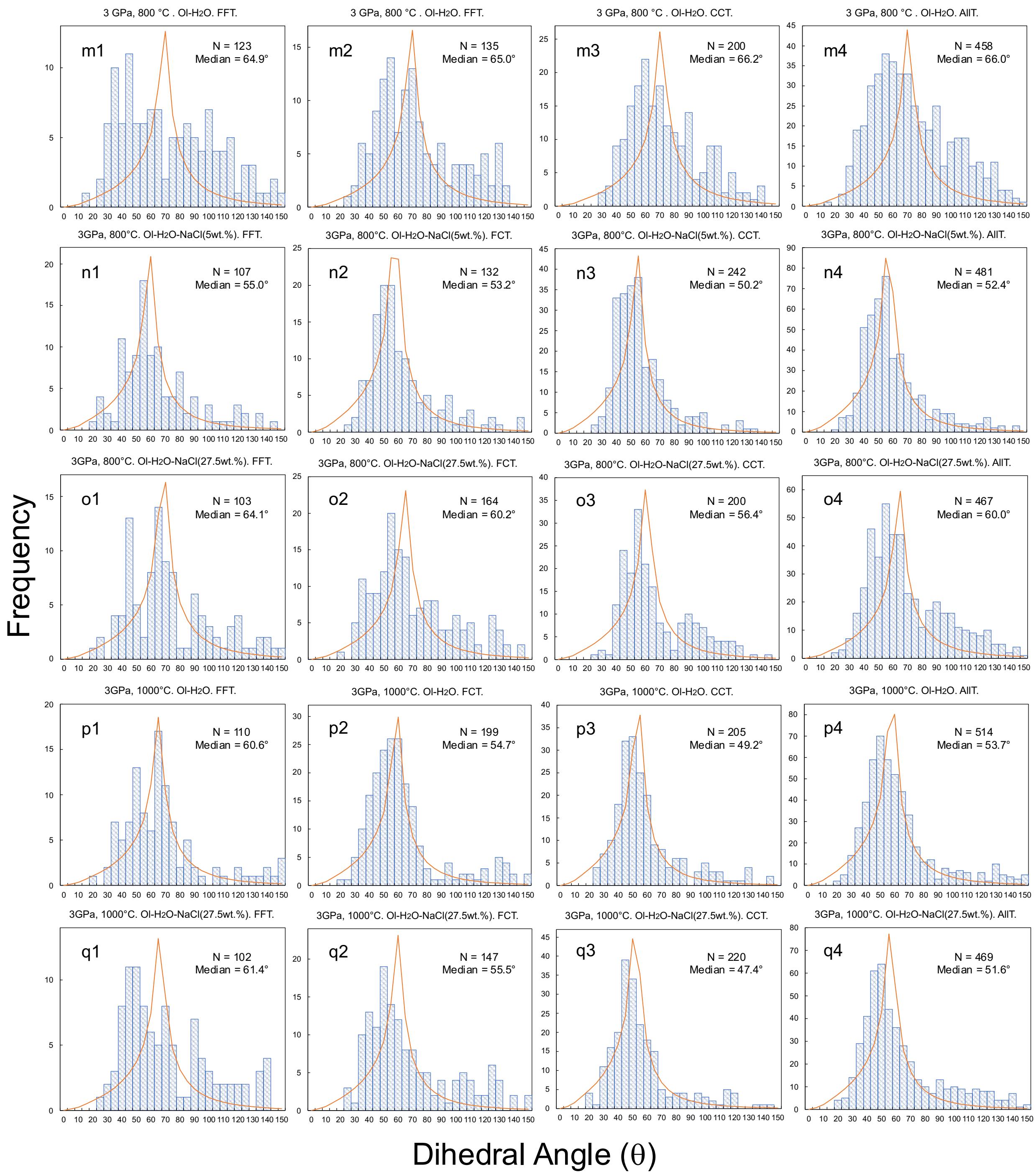

Figure S5. Frequency distribution histograms of measured apparent dihedral angles (θ) in olivine–fluid systems at 1–3 GPa and 800–1100 °C. Theoretical distributions (orange curves) for the mono–mineralic and isotropic systems are also shown in the histograms along with the median values (Jurewicz & Jurewicz, 1986). The P–T and fluid composition are shown for each system. Abbreviations: ol=olivine, FFT = faceted–faceted type angle, FCT = faceted–curved type angle, CCT= curved–curved type angle, AllT= all type of measured angle.

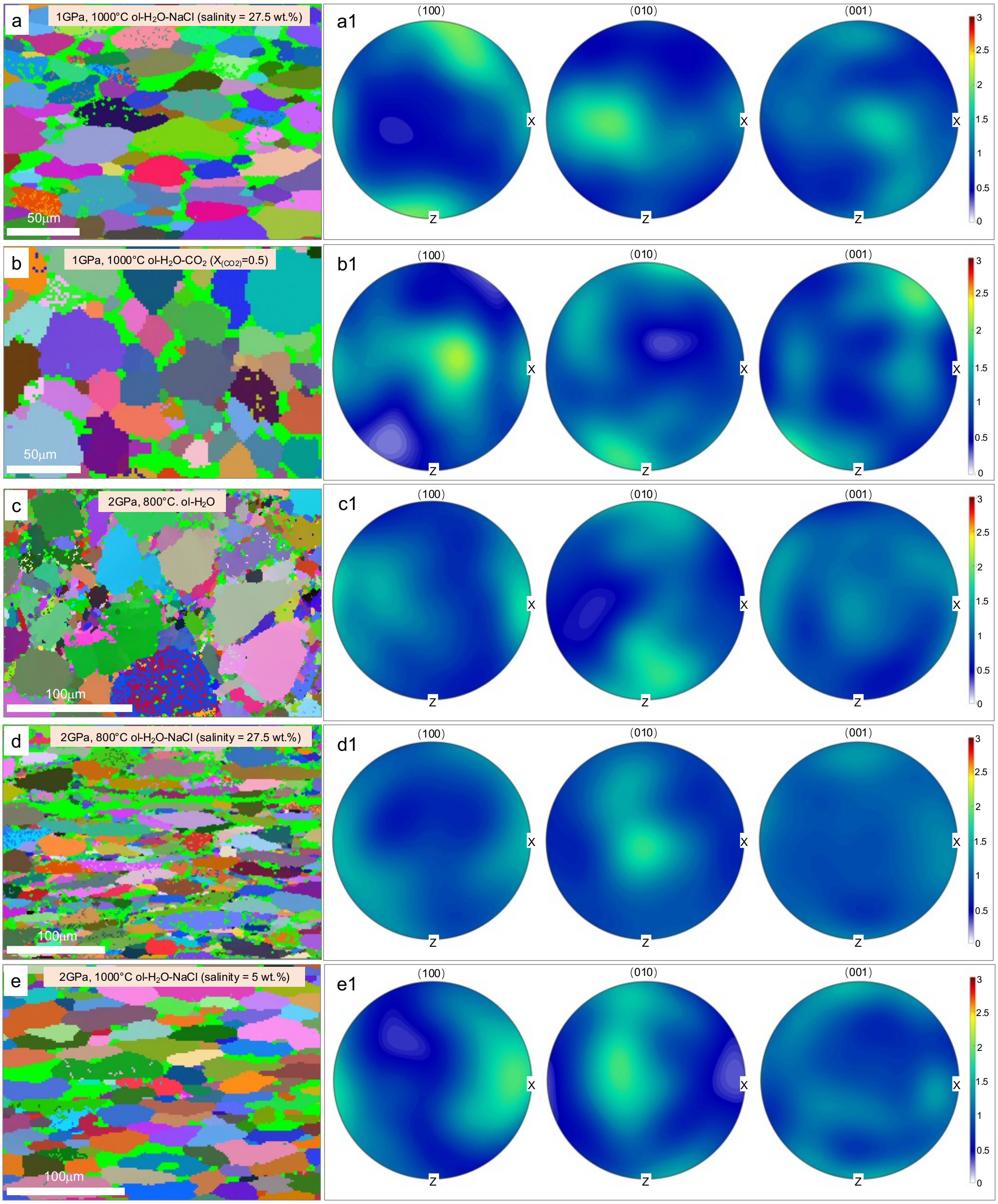

Figure S6. EBSD maps and corresponding Pole figures under static compression conditions. a–e, EBSD maps of recovered olivine aggregate in olivine–fluid systems. The small points within grain are attributed to the noise, crystal defects, and fluid inclusions, which are mostly removed via denoise processes while making pole figure. The crack in c was formed during the decompression, and the mapping direction was calibrated during the EBSD data process. In these systems, all grains are olivine with different orientations. **a1–e1**, Pole figures to show the crystallographic orientation of (100), (010), and (001) corresponding to a–e. The intensities in the color bar are in multiples of the random distribution. The P–T condition and fluid composition are shown along with the corresponding system. Abbreviation: ol=olivine.

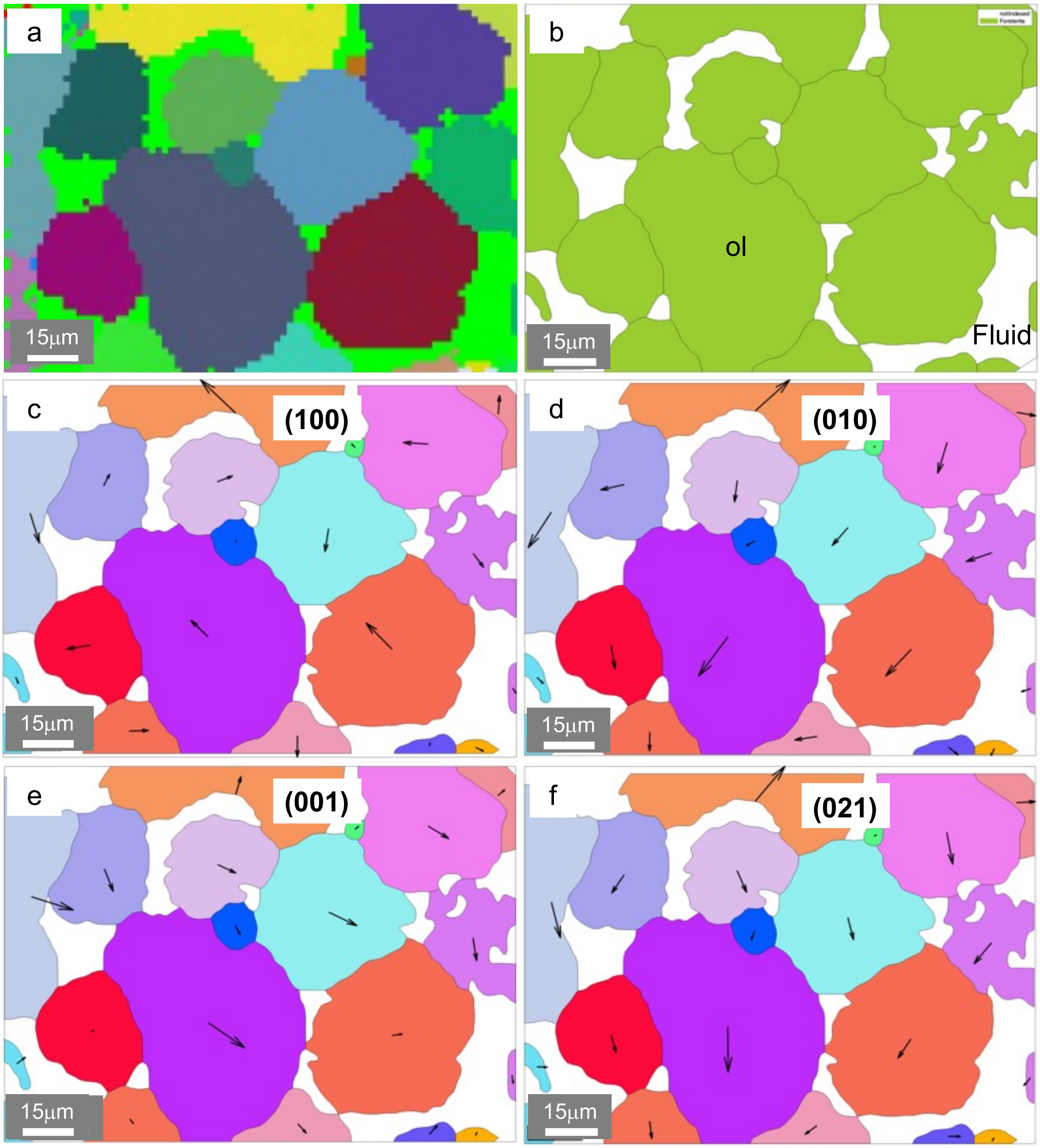

Figure S7. EBSD data and olivine orientation in the H2O system at 1 GPa and 1000°C. a, EBSD map with denoise process. **b**, Grain image reconstruction produced by MTEX toolbox in MATLAB. **c–f**, Special crystal orientation in 2–D grain image given by MTEX toolbox in MATLAB. The orientation is shown for each system. The orientations sometime seem similar or overlapped in 2–D image, it is necessary to check the 3–D spatial orientation while compilation. All grains in figure are olivine.

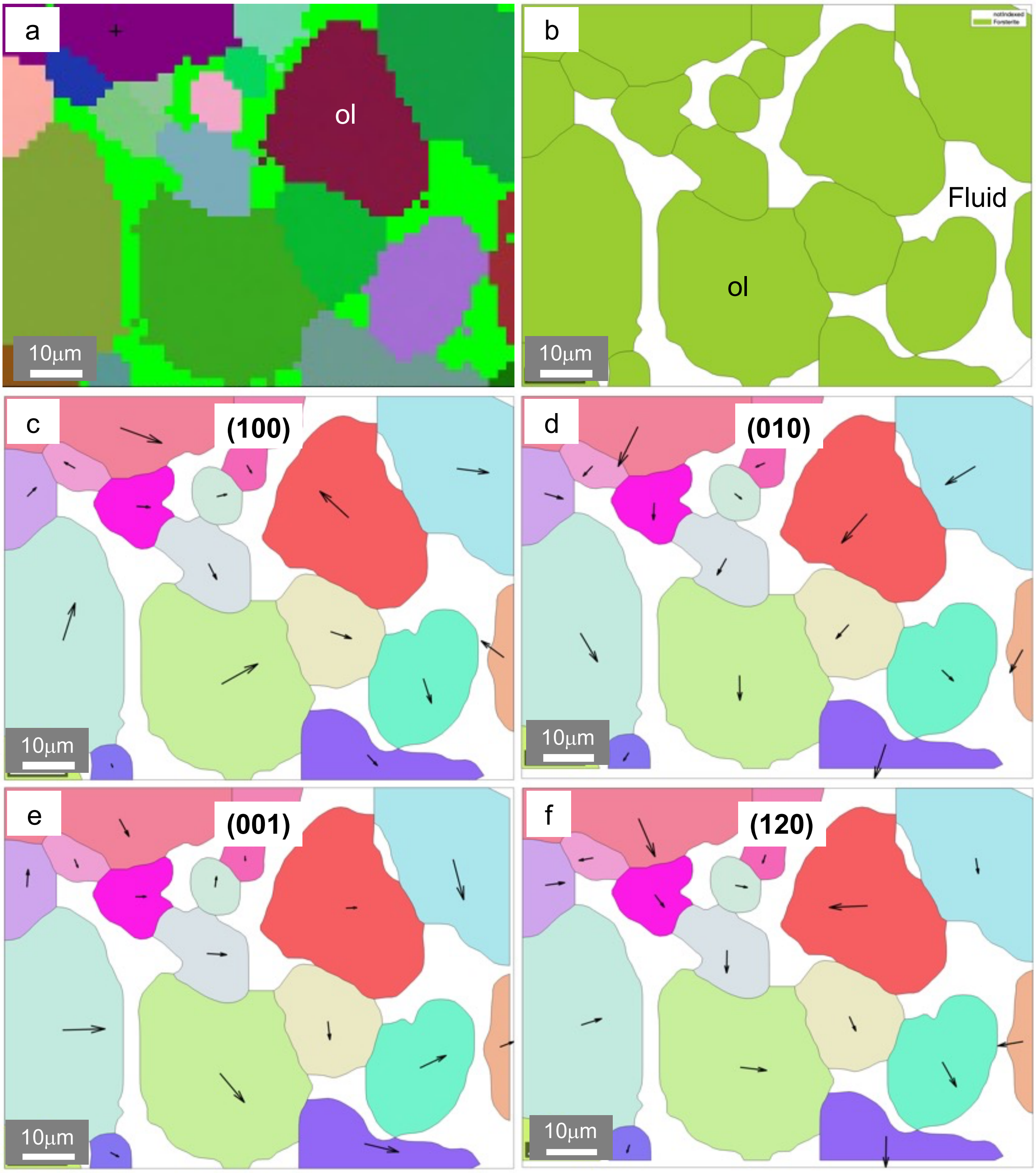

Figure S8. EBSD data and olivine orientation in the H_2O–CO_2($X_{(CO2)}$=0.5) system at 1 GPa and 1000°C. **a**, EBSD map with denoise process. **b**, Grain image reconstruction produced by MTEX toolbox in MATLAB. **c–f**, Special crystal orientation in 2–D grain image given by MTEX toolbox in MATLAB. The orientation is shown for each system. The orientations sometime seem similar or overlapped in 2–D image, it is necessary to check the 3–D spatial orientation while compilation. All grains in figure are olivine.

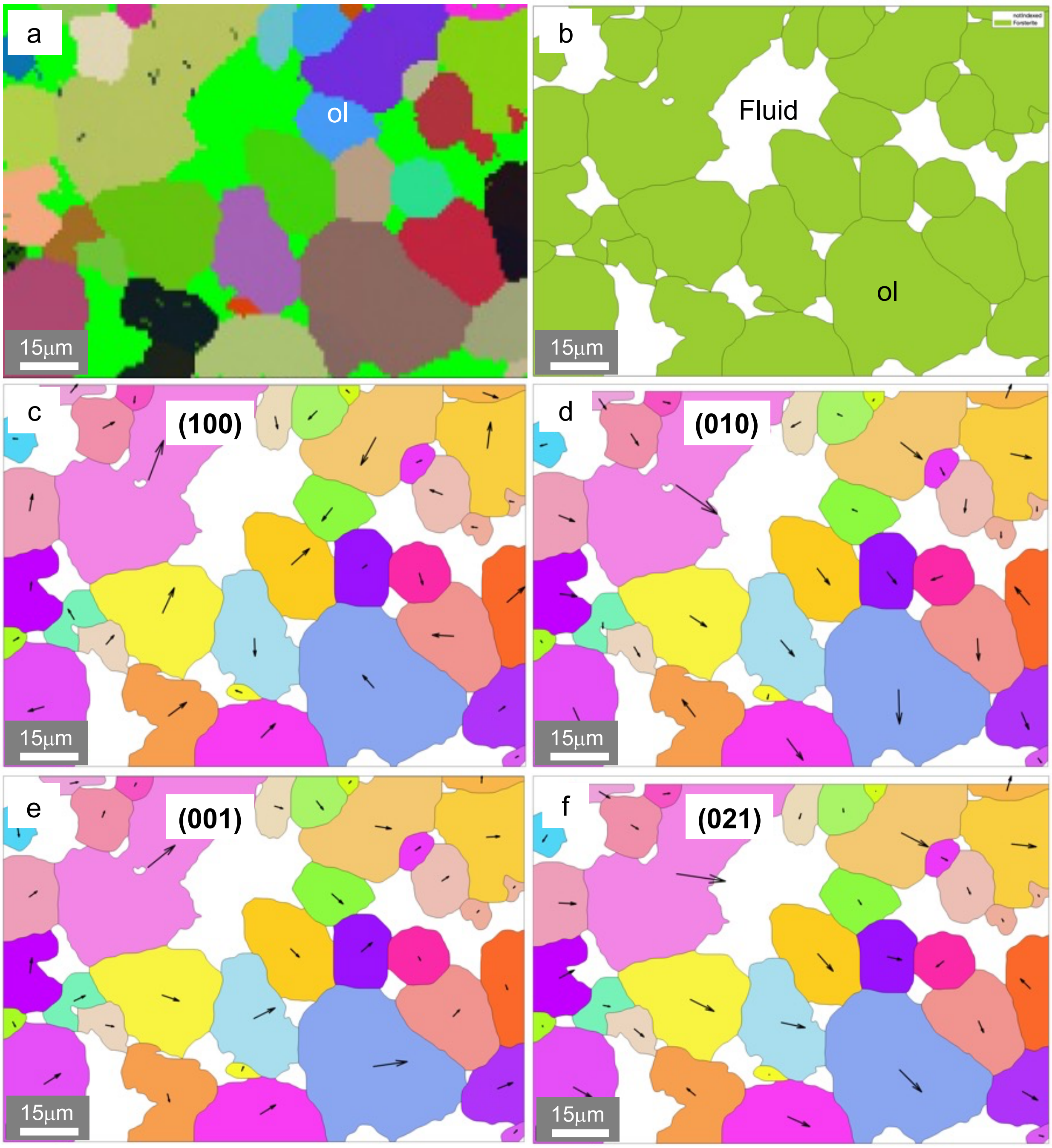

138 **Figure S9. EBSD data and olivine orientation in the H_2O system at 2 GPa and 1000°C. a**, EBSD map
139 with denoise process. **b**, Grain image reconstruction produced by MTEX toolbox in MATLAB. **c–f**,
140 Special crystal orientation in 2–D grain image given by MTEX toolbox in MATLAB. The orientation is
141 shown for each system. The orientations sometime seem similar or overlapped in 2–D image, it is
142 necessary to check the 3–D spatial orientation while compilation. All grains in figure are olivine.

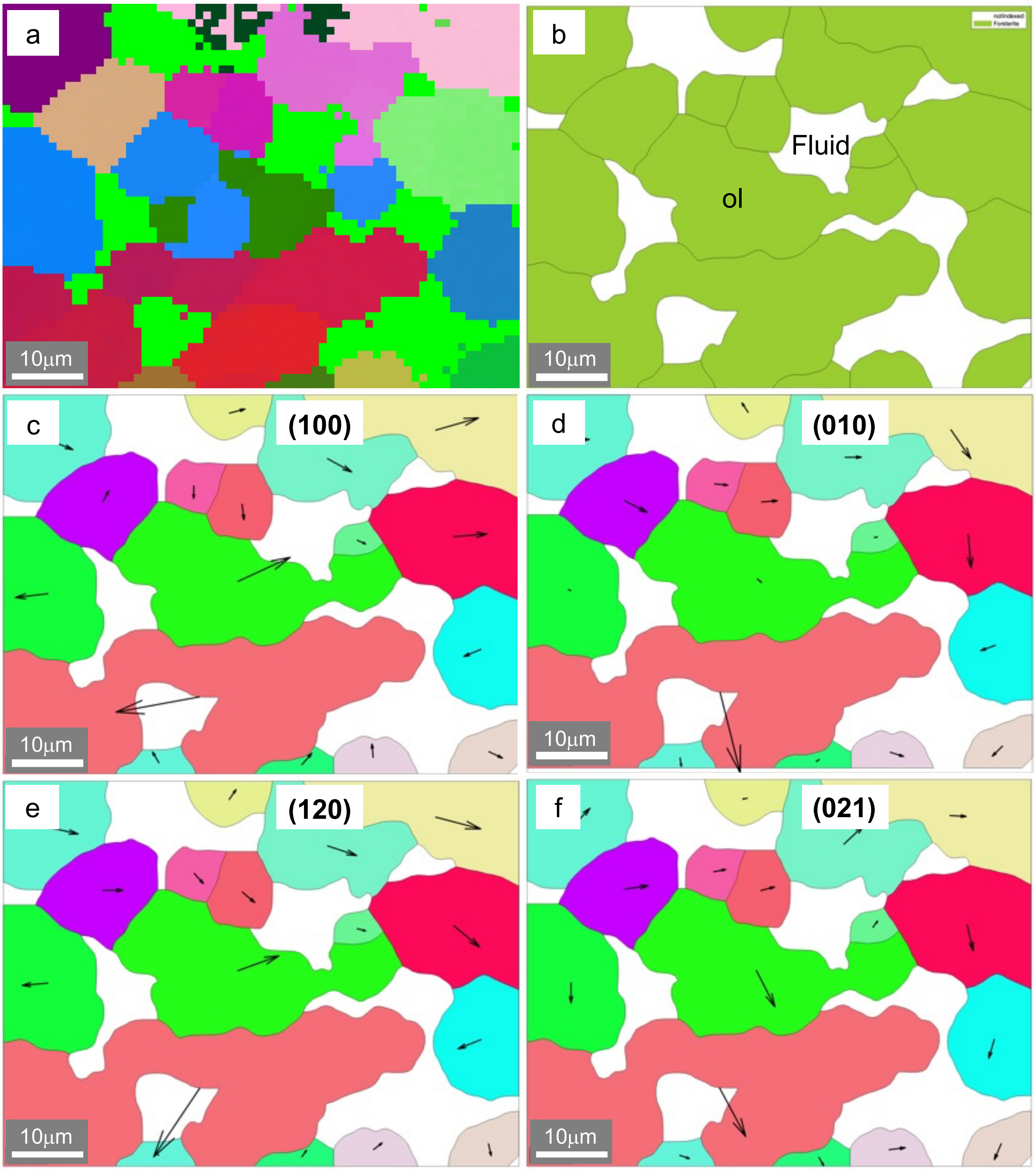

Figure S10. EBSD data and olivine orentation in the H_2O–NaCl (27.5wt%) system at 2 GPa and 1000°C. **a**, EBSD map with denoise process. **b**, Grain image reconstruction produced by MTEX toolbox in MATLAB. **c–f**, Special crystal orientation in 2–D grain image given by MTEX toolbox in MATLAB. The orientation is shown for each system. The orientations sometime seem similar or overlapped in 2–D image, it is necessary to check the 3–D spatial orientation while compilation. All grains in figure are olivine.

3. Table 1. List of calculated FF–type dihedral angles formed by low–Miller Index grain boundary planes and interfaces with fluid at a triple junction

Grain Boundary Plane	Faceted Interface	C1 \ C2	25.0	43.0	38.5	47.0	40.7	66.2	55.1	51.5	44.8	Flat face
100	110	25.0	**50.0***	68.0	63.5	72.0	65.7	91.2	80.1	76.5	69.8	25.0
100	120	43.0	68.0*	**86.0**	81.5	90.0	83.7	109.2	98.1	94.5	87.8	43.0
100	101	38.5	63.5*	81.5*	**77.0***	85.5	79.2	104.7	93.6	90.0	83.3	38.5
010	120	47.0	72.0	90.0	85.5	**94.0**	87.7	113.2	102.1	98.5	91.8	47.0
010	021	40.7	65.7*	83.7	79.2*	87.7	**81.4***	106.9	95.8	92.2	85.5	40.7
101	021	66.2	91.2	109.2	104.7	113.2	106.9	**132.4**	121.3	117.7	111	66.2*
101	120	55.1	80.1*	98.1	93.6	102.1	95.8	121.3	**110.2**	106.6	99.9	55.1*
101	001	51.5	76.5*	94.5	90.0	98.5	92.2	117.7	106.6	**103**	96.3	51.5*
101	110	44.8	69.8*	87.8	83.3	91.8	85.5	111.0	99.9	96.3	**89.6**	44.8

Bold represents symmetric configuration.

The star superscript represents calculated angles that are consistent with experimental data.